PAPER

Check for updates

Theoretical screening of single atom doping on β-Ga₂O₃ (100) for photoelectrochemical water splitting with high activity and low limiting potential†

Sijia Fu,[a] David Lewis,[a] Philip van Eyk, [ID] [a] Petar Atanackovic[b] and Yan Jiao [ID] *[a]

Photoelectrochemical (PEC) water splitting combined with renewable energy is an appealing approach for solar energy conversion and storage. Monoclinic gallium oxide (β-Ga₂O₃) has been identified as a promising photoelectrode for PEC because of its good electrical conductivity and chemical and thermal stability. However, the wide bandgap (around 4.8 eV) and the recombination of photogenerated electrons and holes inside β-Ga₂O₃ limit its performance. Doping β-Ga₂O₃ is a practical strategy to enhance photo-catalytic activity, but studies on doped β-Ga₂O₃ based photoelectrodes are lacking. In this study, we evaluate the doping effect of ten different dopants for β-Ga₂O₃ photoelectrode at the atomic level using density functional theory calculations. In addition, the oxygen evolution performance is evaluated on doped structures as it is considered the bottleneck reaction in water slitting on the anode of the PEC cell. Our results suggest that rhodium doping is optimal as it demonstrated the lowest overpotential for oxygen evolution reaction. We performed further electronic structure analysis, indicating the narrower bandgap and enhanced photogenerated electron–hole transfer comparing with β-Ga₂O₃ are the main reasons for the improved performance after Rh doping. This study demonstrates that doping is an attractive strategy for the development of efficient Ga₂O₃-based photoanodes and it will be of great importance in helping the design of other semiconductor-based photoelectrodes for practical application.

Introduction

Converting solar energy into sustainable fuels by artificial photosynthesis is highly desirable to help meet the increasing global energy demand and to alleviate the environmental issues caused by fossil fuels consumption.[1] Photoelectrochemical (PEC) water splitting has long been considered a promising method to obtain carbon-free solar fuel from water.[2] Typically, photoactive and durable semiconductors are used as photoanodes as they can absorb sunlight to generate electron–hole pairs to execute the redox reactions.[3] The current bottleneck in the commercialization of PEC cells is the long term instability of photoelectrodes and the low efficiency of the system.[4] Up to now, significant research effort has been devoted to improve the efficiency and reliability of PEC cell. However, seeking for new,

proficient, and steady photoanodes capable of oxidising water to oxygen remains the key to achieving excellent energy conversion performance in PECs.

Various semiconducting oxides have been studied as photoelectrodes for PEC, such as TiO₂, Fe₂O₃, RuO₂, and ZnO.[5–7] Ga₂O₃ is electrically conducting and it has attracted much attention in many areas, such as transparent conductors and ultraviolet (UV) photodetectors.[8–10] Moreover, among the five distinct crystalline structures of Ga₂O₃ (α, β, γ, δ, and ε), monoclinic gallium oxide (β-Ga₂O₃) is the most stable crystal phase, and β-Ga₂O₃ is a chemically, thermally, and catalytically stable native oxide,[11] and has higher photocatalytic activity than the other phases.[8] Therefore, β-Ga₂O₃ is an excellent material to be used as photoelectrode for PEC water splitting. For example, Oshima *et al.* used the single crystalline β-Ga₂O₃ as the photoelectrode with efficient photoelectrolysis of water.[12] They found that the incident photon-to-current conversion efficiency was 36% at the illuminated edge of 5.2 eV.[12] Stoichiometric water splitting occurred when an external bias of 1 V was applied.[12] Inspired by this work, Chang *et al.* created Radio Frequency sputtered Ga₂O₃ films for PEC water splitting, that also had good stability as no decomposition and/or corrosion occurred on the surface of Ga₂O₃ films.[13] He

[a]*School of Chemical Engineering and Advanced Materials, Faculty of Science, Engineering and Technology, The University of Adelaide, Adelaide, South Australia, 5005, Australia. E-mail: yan.jiao@adelaide.edu.au*
[b]*Silanna picoFAB Facility, The University of Adelaide, Adelaide, South Australia, 5005, Australia*
†Electronic supplementary information (ESI) available. See DOI: https://doi.org/10.1039/d3nr00149k

et al. synthesized Ga_2O_3 nanorods with an oval-like profile, which possessed enhanced performance than high-crystalline Ga_2O_3 nanorods with a photo-current density of 122.4 $\mu A\ cm^{-2}$ at 0.6 V *vs.* Ag/AgCl.[14] These studies demonstrate that Ga_2O_3 is a promising material for photoelectrodes in PEC. However, the inherent drawbacks of Ga_2O_3 is that its wide band gap (4.8 eV) makes it sensitive to only UV region of the solar spectrum and the recombination of photogenerated electrons and holes, which were also the issues highlighted in the aforementioned experiments.[15]

Doping has been shown to be an efficient method not only to narrow the bandgap for photoelectrodes, but also to increase the photocatalytic activity by enhancing the visible light absorption.[16–21] More importantly, the bulk carrier recombination can be restricted by doping, hence photoexcited charge carriers can migrate to the surface efficiently to participate the reactions.[22] Developing β-Ga_2O_3 based photoelectrodes by doping with other elements could open up new opportunities for high activity and low overpotential. Some researchers have studied the structures and photocatalysis applications of doped gallium oxide based materials, as summarized in Table S1 of ESI.† For example, Sakata found that by adding Zn ions, the photocatalytic activity of Ga_2O_3 was improved for overall water splitting.[18,20] A computational study further confirmed that introducing Zn on β-Ga_2O_3 can enhance the absorption and reflectivity of β-Ga_2O_3 in the near infrared region.[23] However, more than half of the studies summarizing in Table S1† are experimental works, containing various photocatalytic reactions, such as hydrogen production, CO_2 reduction, and harmful volatile organic compounds removal. Moreover, only a few dopant types were studied. For the computational works, seldom of them consider oxygen evolution reaction (OER), which is regarded as the bottleneck reaction in water splitting that occurs at the anode for PEC water splitting.[1] Additionally, there were no systematic computational studies on doped β-Ga_2O_3 based photoelectrodes to screen the most suitable dopant yet.

In this work, we screened ten different elements (Si, Co, Ni, Cu, Zn, Ru, Rh, Sn, Pt, and Au) as possible substitutional dopants of Ga atom. (100)-B type, as the most stable surface of β-Ga_2O_3, is selected as the surface for doping.[24,25] We studied the doping structures and their thermodynamic stability at the atomic level by means of density functional theory (DFT) calculations. Doped β-Ga_2O_3 is used as a photoanode in PEC cells. We also analysed the reaction activity of OER on these doping surface structures, finding Rh doping had the best performance. We further demonstrated the changes on band structures, density of states (DOS), and charge density distribution after Rh doping. We found that the improved OER performance after Rh doping could be explained by the narrower band gap and the effective separation of photogenerated electrons and holes pairs. The significance of this research is to provide guidelines for designing Ga_2O_3 based photoelectrodes.

Computational method

All calculations were carried out using DFT, as implemented in the Vienna *Ab initio* Simulation Package (VASP).[26–30] The electronic exchange–correlation effects were represented by the Perdew–Burke–Ernzerhof (PBE) functional within the generalized gradient approximation (GGA).[29] The projector augmented wave (PAW) method was used with a kinetic cutoff energy of 420 eV. A $1 \times 4 \times 2$ supercell containing 160 atoms is applied to model the doped structures on (100) facet of β-Ga_2O_3, in which a Ga atom on the surface is substituted by one dopant atom. This corresponds to a doping concentration of 1.7 wt%. A vacuum thickness of 10 Å in the *z*-direction was applied to avoid interactions caused by the periodic boundary conditions. For the Brillouin zone integration, a Monkhorst–Pack set of $4 \times 8 \times 6$ *k*-points was applied. Moreover, the generalized gradient approximation (GGA) and Heyd–Scuseria–Ernzerhof (HSE06) hybrid exchange–correlation functional were used to calculate the band gaps on the basis of optimized structures.[31] The electronic band calculations were performed by post-processing VASPKIT package.[32] The details of the GGA band structures of Ga_2O_3 and all doping structures are summarized in Fig. S1 and S2 within the ESI,† respectively.

The formation energy of Ga vacancy is calculated by

$$\Delta E^f = E_{defect} - E_{perfect} + \sum n_i\mu_i \qquad (1)$$

where E_{defect} is the total energy of the supercell with defect, $E_{perfect}$ is the total energy of perfect intrinsic supercell, respectively, n_i represents the number of atom (*i*) removed from the perfect supercell, and μ_i denotes the chemical potential of the corresponding atom.

To evaluate the thermodynamic stability of the doped structure, the binding energy (E_b) was calculated as

$$E_b = E_{substrate\text{-}dopant} - E_{substrate} - E_{BULK}/n \qquad (2)$$

where $E_{substrate\text{-}dopant}$ and $E_{substrate}$ are the total energies of the substrate-dopant and substrate, respectively. E_{BULK} is the energy of the metal in the bulk.
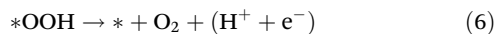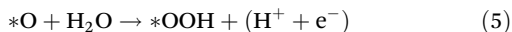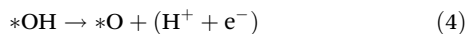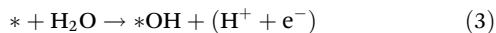
Associate Professor Yan Jiao is an ARC Future Fellow at the University of Adelaide's School of Chemical Engineering. She leads the Energy Materials Computation Research Group. She completed her PhD at the University of Queensland in 2012 and later joined the University of Adelaide, where she progressed from Research Fellow to Associate Professor. Recognized as a Young Tall Poppy and one of The Australian's 40 Rising Stars, her multidisciplinary research focuses on designing efficient energy materials for the storage and conversion of clean energy with a core strength in molecular modelling.

Yan Jiao

The OER performance on the doped β-Ga_2O_3 is studied *via* the four-electron pathway based on the computational hydrogen electrode model.[33] These four elementary steps of OER are

$$* + H_2O \rightarrow *OH + (H^+ + e^-) \quad (3)$$

$$*OH \rightarrow *O + (H^+ + e^-) \quad (4)$$

$$*O + H_2O \rightarrow *OOH + (H^+ + e^-) \quad (5)$$

$$*OOH \rightarrow * + O_2 + (H^+ + e^-) \quad (6)$$

in which * denoted dopant-Ga_2O_3. The free energy of O_2 gas is obtained from the experimental Gibbs free energy of the reaction $2H_2O(l) \rightarrow O_2(g) + 2H_2(g)$ (4.92 eV) at the standard condition.[34] In addition, the free energy of the $(H^+ + e^-)$ pair is referenced to the chemical potential of gaseous H_2 under standard conditions (0 V *versus* standard hydrogen electrode, at 101 325 Pa). Accordingly, the free energy change of each step can be written as

$$\Delta G_1 = \Delta G_{*OH} \quad (7)$$

$$\Delta G_2 = \Delta G_{*O} - \Delta G_{*OH} \quad (8)$$

$$\Delta G_3 = \Delta G_{*OOH} - \Delta G_{*O} \quad (9)$$

$$\Delta G_4 = 4.92 - \Delta G_{*OOH} \quad (10)$$

where ΔG_{*OH}, ΔG_{*O}, and ΔG_{*OOH} are the adsorption energies of *OH, *O, and *OOH. These adsorption energies are defined as

$$\Delta G_{*OH} = G_{*OH} - G_* - (G_{H_2O} - 1/2G_{H_2}) \quad (11)$$

$$\Delta G_{*O} = G_{*O} - G_* - (G_{H_2O} - G_{H_2}) \quad (12)$$

$$\Delta G_{*OOH} = G_{*OOH} - G_* - (2G_{H_2O} - 3/2G_{H_2}) \quad (13)$$

where the G_*, G_{*OH}, G_{*O}, and G_{*OOH} are the free energies of *, *OH, *O, and *OOH, respectively. G_{H_2O} and G_{H_2} are the free energies of H_2O and H_2 molecules, respectively.

The Gibbs free energy (G) is calculated by

$$G = E + ZPE - TS + G_U \quad (14)$$

in which E indicated the electronic energy obtained from DFT calculations.[35] TS and ZPE indicate entropy and zero-point energy corrections, and T is the room temperature ($T = 298.15$ K). ZPE and vibrational entropy of adsorbed species were calculated from vibrational frequencies.[36] Entropies of gas molecules (H_2 and CO_2) were taken from standard values.[37] G_U is the electrode potential and the value is $-n_eU$, where n_e indicated the number of electrons and U is the electrode potential. Among the four OER steps, the step with the highest increasing energy is regarded as the potential-determining step (PDS). The OER overpotential (η_{OER}) can be used to evaluate the catalytic activity, and a lower η_{OER} indicated better OER activity. η_{OER} is defined as

$$\eta_{OER} = max(\Delta G_1, \Delta G_2, \Delta G_3, \Delta G_4)/e - 1.23 \quad (15)$$

Results and discussion

Stability and structure of doped Ga_2O_3

The structure of bulk β-Ga_2O_3 is shown in Fig. 1a. There are two non-equivalent Ga sites and three non-equivalent O sites in bulk β-Ga_2O_3.[38–40] Ga1 is bound to four O anions in a form of distorted tetrahedron, while Ga2 is formed by binding with six O anions octahedrally. The (100)-β surface with fourfold coordinated Ga1 and fivefold coordinated Ga2 is shown in Fig. 1b. The O1 site is three-fold coordinated, with one Ga1 and two Ga2. O2 is also three-fold coordinated, but with two Ga1 and one Ga2. The O3 site is four-fold coordinated, with one Ga1 and three Ga2. The optimized lattice parameters for β-Ga_2O_3 are $a = 12.45$ Å, $b = 3.08$ Å, $c = 5.88$ Å, and $\beta = 103.70°$, which agree well with both experimental and other DFT values.[41–43]

On the (100) surface, bond lengths of Ga2–O (1.92 Å) are longer than those of Ga1–O (1.88 Å). Moreover, the calculated vacancy formation energy for Ga2 and Ga1 is 9.23 eV and 12.36 eV, respectively. These values are consistent with other reported values for Ga2 vacancy formation energy.[44,45] Therefore, it is easier for dopants to replace Ga2 rather than Ga1.[46] We then considered the doped structure by introducing dopants at the Ga2 position for the ten different elements. One Ga2 atom in the supercell is replaced with one dopant.
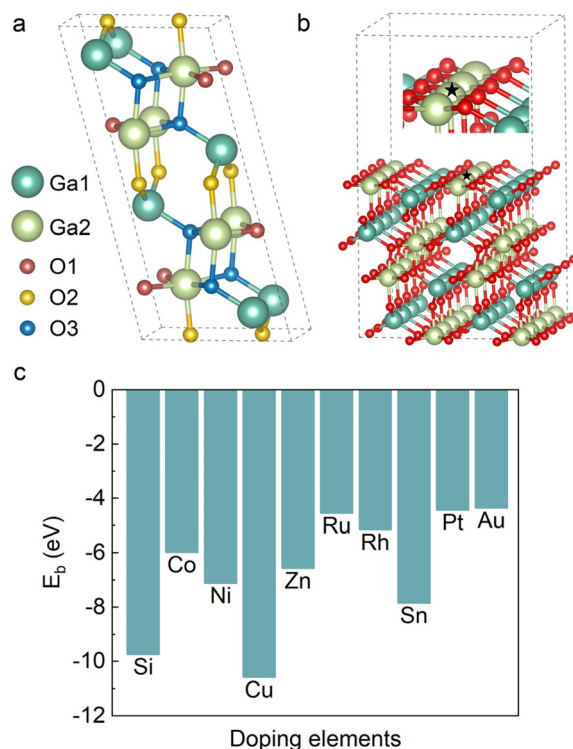

Fig. 1 (a) Schematic representation of the unit cell of β-Ga_2O_3. (b) Schematic representation of (100) β-Ga_2O_3 surface. Colour code: Ga1, dark green; Ga2, light green; O, red. The star indicates this Ga will be substituted by other elements. (c) The binding energy (E_b) of various elements on the (100) β-Ga_2O_3 surface.

The doping local structure is presented in Fig. 1b, and the Ga2 position being substituted by various doping elements is highlighted with the star.

The thermodynamic stability of the doped structures are evaluated by calculating the binding energy (E_b) of various elements.[47] A negative E_b indicates that the structure is thermodynamically stable.[47] As shown in Fig. 1c, our results indicated that the doped structures all have a negative binding energy, which indicates they are all stable structures. This is because the doping elements have the similar ionic radii with Ga ion (62 pm).[48]

The calculated local structures around dopant for every doped structure and the bond distance after doping are also summarized in Fig. S3,† showing no obvious distortion. The dopants in Ga_2O_3 lattice only distorts the local geometry and does not impact the geometry beyond the next nearest Ga cations. In conclusion, the doping structures are thermodynamically stable.

Catalytic performance evaluation of β-Ga_2O_3 doping structures to OER

To evaluate OER performance on various doping structures, we investigate the intermediate species involved (*OH, *O, and *OOH), and the free energies of most stable configurations are listed in Table S1.† The free energy change of each step on both the doping structures and the clean (100) β-Ga_2O_3 facet are calculated based on eqn (6) to (9). The OER free energy diagrams are plotted in Fig. 2a. The computational results demonstrate that most of the steps are uphill when no potential bias is applied. For the clean (100) surface, the PDS is the second step (*OH → *O), with an energy difference of 4.85 eV. It can be observed that comparing to undoped clean (100) β-Ga_2O_3 surface, doping enhance activity. The free energy diagrams at standard equilibrium potential for oxygen evolution at $U = 1.23$ V is presented in Fig. 2b. For most of the doping structures, the OER process is impeded by the process of *OH → *O with an uphill free energy change over 1 eV. Only for Ru doping structure, the fourth step (*OOH → * + O_2) is hindered with a free energy change of 1.29 eV. The overpotentials of OER (η_{OER}) are summarized in Fig. 2c, as calculated by eqn (14). Among all doping structures, it can be seen that Rh doped β-Ga_2O_3 shows relatively best OER activity with the lowest OER overpotential ($\eta_{OER} = 0.50$ V).

Since the above calculations are based on elements substituting on Ga2 site, we also considered Rh doping on the Ga1 site to compare the OER performance difference. Rh doping on Ga1 and
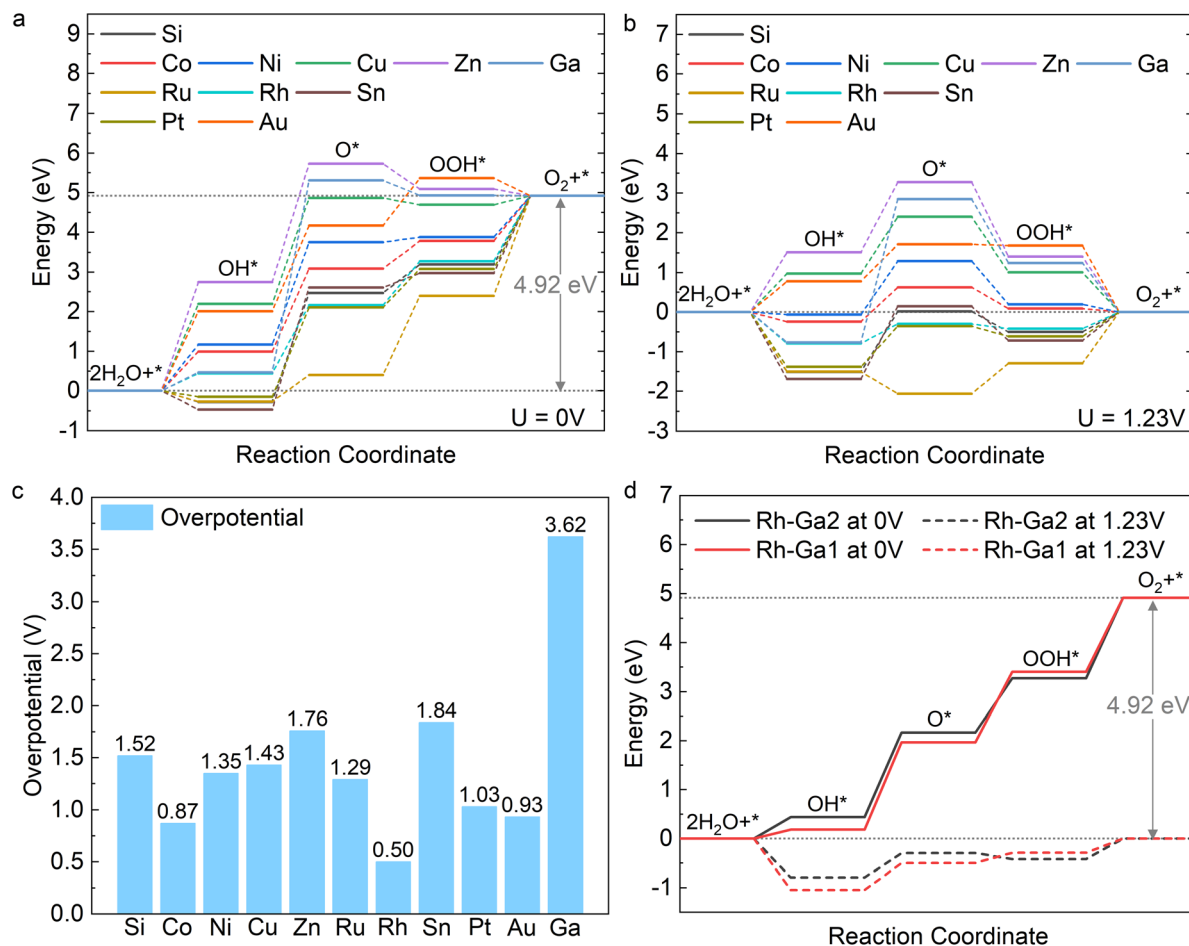

Fig. 2 The free energy diagrams for OER on all doping structures and clean (100) β-Ga_2O_3 facet at (a) zero cell potential ($U = 0$ V), and (b) the equilibrium potential ($U = 1.23$ V). (c) The overpotential of all doping elements. (d) The free energy diagrams for Rh−Ga2 and Rh−Ga1 at $U = 0$ and 1.23 V.

Ga2 are labelled as Rh–Ga1 and Rh–Ga2, respectively. The free energy diagrams for Rh-Ga1/Ga2 at U = 0/1.23 V are plotted in Fig. 2d. At U = 1.23 V, some of the steps become downhill but some steps remain uphill. Specifically, the first and the third step for Rh–Ga2 are downhill, while only the first step for Rh–Ga1 is downhill. The overpotential for Rh–Ga2 (0.50 V) is 0.12 V less than that for Rh–Ga1 (0.62 V). This may because for Rh–Ga1, the neighbouring Ga1 atom tend to bind the intermediates (*OH and *O) with Rh together, causing a stronger binding strength. To sum up, Rh–Ga2 possesses the best OER performance owing to its moderating binding with the reaction intermediates.

Electronic structure of Rh doped β-Ga₂O₃

We further calculated the electronic structures for β-Ga₂O₃ and Rh doped β-Ga₂O₃ to further explore the change of the band structures, total density of states (TDOS), and project density of states (PDOS) after doping. We obtained the band structure, whose behaviour will be discussed referring to the high symmetry path in the Brillouin zone as $V–Z–\Gamma–A–M–L$ (see Fig. 3a).[49] The first principle calculations of the electronic band structure of β-Ga₂O₃ unit cell and Rh doped β-Ga₂O₃ by HSE06 are presented in the left of Fig. 3b and c, respectively.
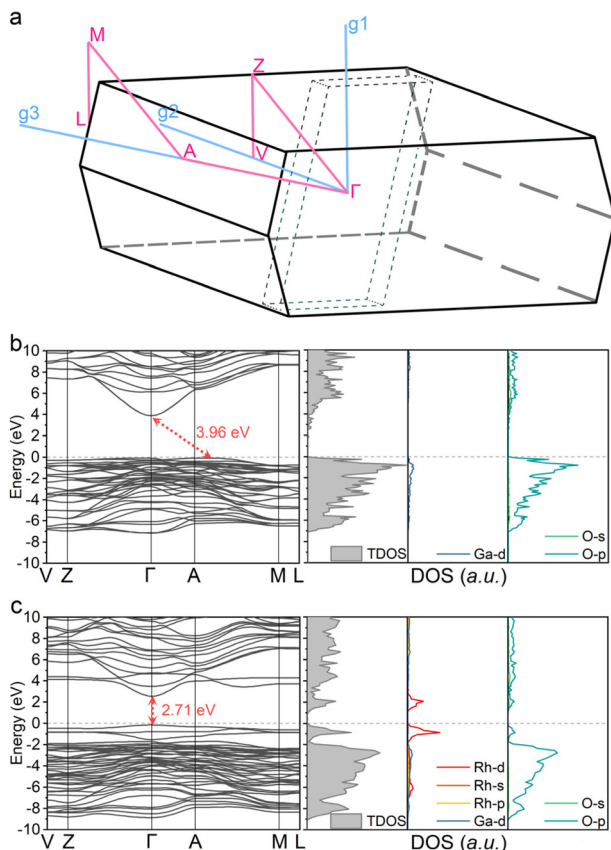
The Fermi level is adjusted to be at 0 eV, representing by a vertical dashed line. Here, the calculation indicates β-Ga₂O₃ has the indirect band gap with the gap value of 3.96 eV, which is more accurate than its GGA result (1.91 eV, Fig. S1 of ESI†). The conduction band minimum (CBM) is located at the Γ point and the valence band maximum (VBM) is located during $V–M$ region, which is consistent with the results of other researchers' work.[50] After Rh doping, the bandgap is narrowed to 2.71 eV, as shown in Fig. 3c. Moreover, the Rh-doped β-Ga₂O₃ has a direct bandgap with the VBM and CBM both located on Γ point. It should be noticed that this is a unit cell, containing one Rh atom, 11 Ga atoms, and 18 O atoms. The narrowing band gap indicates that the utilization ratio of solar energy for water splitting can be improved to some degree by the doped Rh. In addition, the calculated bandgap reveals that the absorption edge of Ga₂O₃ can be extended to 457 nm, which is in the visible light region (400 to 800 nm).[51]

In order to study the effect of doping Rh on the electronic structure of support, the corresponding TDOS and PDOS are calculated and displayed in the right part of Fig. 3b and c. It is found that the major component for the valence bands of Ga₂O₃ is the O p orbital, while the Ga d and p orbitals are negligible. On the other hand, both Ga and O contribute to the conduction bands. While for Rh-doped β-Ga₂O₃, impurity states are found to appear above VBM by 1.24 eV. CBM level is slightly shifted in the downward direction, resulting in a bandgap narrowing to 2.71 eV. Moreover, the top of the valence band is attributed to the overlap of Rh d and O p states. Because of the lower electro-negativity of Rh, more electron densities around Rh are transferred to the nearest neighbour O atoms, forming the PDOSs of O p states near the top of the valence band. To sum up, the DOS analysis indicates that the impurity states are mainly contributed by the d states of Rh, which shift the CBM edge at lower energy and reduce the bandgap.

To further understand the generation and transportation of the electron–hole pairs, we calculated the composition of the charge densities of CBM and VBM states for both β-Ga₂O₃ and Rh doped β-Ga₂O₃. Fig. 4a shows the partial charge density cal-
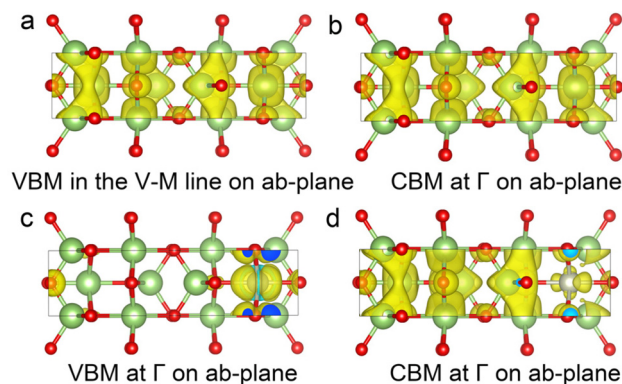

Fig. 3 (a) The high symmetry pathway of β-Ga₂O₃ in the Brillouin zone. The K points are $V = \left(0\frac{1}{2}0\right)$, $Z = \left(\frac{1}{2}\frac{1}{2}0\right)$, Γ = (000), $A = \left(0\frac{1}{2}\frac{1}{2}\right)$, $M = \left(\frac{1}{2}\frac{1}{2}\frac{1}{2}\right)$, $L = \left(0\frac{1}{2}\frac{1}{2}\right)$. Band structures by HSE06, calculated TDOS and PDOS of (b) β-Ga₂O₃ and (c) Rh doped β-Ga₂O₃. The top of the valence band is aligned to zero.

Fig. 4 Partial charge density distribution at (a) the top of the valence band in the $V–M$ line and (b) the CBM at Γ point on ab-plane for β-Ga₂O₃. Partial charge density distribution at (c) the VBM at Γ point and (d) the CBM at Γ point on ab-plane for Rh doped Ga₂O₃.

culated at the top of valence band in the *V–M* line for Ga$_2$O$_3$, and that at the saddle point of conduction band (*Γ* point). The VBM charge densities mainly spread over O and Ga atoms, which is the same for CBM. The partial charge density distribution of the VBM and CBM of Rh doped β-Ga$_2$O$_3$, which are both located at the *Γ* point is shown in Fig. 4b. The charge distribution for VBM is mainly located at the inner Rh-core, while the oxygen atoms contribute most of CBM. Therefore, for Rh doped structure, the separation of the charge distributions of VBM and CBM will favour the efficient photogenerated electron-holes pairs separation, which is crucial to the PEC cell performance.[52]

Conclusions

In conclusion, first-principles DFT calculations were used to investigate catalytic performance, the geometric and electronic structures of β-Ga$_2$O$_3$ and the ten different elements doped (100)-β surface. First, the doping structures and the stability were confirmed by DFT. After verifying the thermodynamic stability of the doping structures, we demonstrated that the OER activity can be efficiently tailored by doping. Our results suggested that Rh doping possesses the most enhanced OER performance among the ten doping structures. The free energy calculations indicated that the catalytic performance can be enhanced owing to the moderated reaction intermediate adsorption strength. It should be noticed that not all doping elements are promising for OER. Therefore, our study is very important in screening the promising doping candidates and providing properly doping configurations of the efficient catalysts. We further studied the electronic structures of Rh doped β-Ga$_2$O$_3$, and found that the calculated band gap is narrowed and the photogenerated electron–hole pairs separation ability is enhanced, indicating it could present an improved light harvesting performance. Further computational investigations are planned to determine the kinetic parameters of the reaction and experimental works are required to compare with our simulation results. Overall, this study is of great importance for guiding future design of efficient Ga$_2$O$_3$ photoelectrode for water splitting.

Author contributions

Sijia Fu: performed DFT computations, investigation, formal analysis, writing – original draft. Philip van Eyk: supervision, writing – reviewing and editing. David Lewis: supervision, writing – reviewing and editing. Petar Atanackovic: supervision, writing – reviewing and editing. Yan Jiao: conceptualization, resources, supervision, writing – reviewing and editing.

Conflicts of interest

There are no conflicts to declare.

Acknowledgements

References

1 Z. W. Seh, J. Kibsgaard, C. F. Dickens, I. Chorkendorff, J. K. Nørskov and T. F. Jaramillo, *Science*, 2017, **355**(6321), eaad4998.

2 H. Wu, H. L. Tan, C. Y. Toe, J. Scott, L. Wang, R. Amal and Y. H. Ng, *Adv. Mater.*, 2020, **32**, 1904717.

3 J. H. Montoya, L. C. Seitz, P. Chakthranont, A. Vojvodic, T. F. Jaramillo and J. K. Nørskov, *Nat. Mater.*, 2017, **16**, 70–81.

4 W. Yang, R. R. Prabhakar, J. Tan, S. D. Tilley and J. Moon, *Chem. Soc. Rev.*, 2019, **48**, 4979–5015.

5 S. Tanwar, A. Arya, N. Singh, B. C. Yadav, V. Kumar, A. Rai and A. Sharma, *J. Phys. D: Appl. Phys.*, 2021, **55**, 055501.

6 H. Han, F. Riboni, F. Karlicky, S. Kment, A. Goswami, P. Sudhagar, J. Yoo, L. Wang, O. Tomanec and M. Petr, *Nanoscale*, 2017, **9**, 134–142.

7 Y. Kageshima, T. Minegishi, S. Sugisaki, Y. Goto, H. Kaneko, M. Nakabayashi, N. Shibata and K. Domen, *ACS Appl. Mater. Interfaces*, 2018, **10**, 44396–44402.

8 S. Pearton, J. Yang, P. H. Cary IV, F. Ren, J. Kim, M. J. Tadjer and M. A. Mastro, *Appl. Phys. Rev.*, 2018, **5**, 011301.

9 W. Weng, T. Hsueh, S.-J. Chang, G. Huang and H. Hsueh, *IEEE Sens. J.*, 2010, **11**, 999–1003.

10 T. Minami, *J. Vac. Sci. Technol., A*, 1999, **17**, 1765–1772.

11 M. Arunachalam, K. R. Subhash, K.-S. Ahn, C. S. Kim, J.-S. Ha, S.-W. Ryu and S. H. Kang, *ACS Appl. Energy Mater.*, 2022, **5**(2), 2169–2183.

12 T. Oshima, K. Kaminaga, H. Mashiko, A. Mukai, K. Sasaki, T. Masui, A. Kuramata, S. Yamakoshi and A. Ohtomo, *Jpn. J. Appl. Phys.*, 2013, **52**, 111102.

13 S.-J. Chang, Y.-L. Wu, W.-Y. Weng, Y.-H. Lin, W.-K. Hsieh, J.-K. Sheu and C.-L. Hsu, *J. Electrochem. Soc.*, 2014, **161**, H508.

14 W. He, W. Wu, Q. Li, K. Chen and X. Lu, *ChemNanoMat*, 2020, **6**, 208–211.

15 M. Mohamed, C. Janowitz, I. Unger, R. Manzke, Z. Galazka, R. Uecker, R. Fornari, J. Weber, J. Varley and C. Van de Walle, *Appl. Phys. Lett.*, 2010, **97**, 211903.

16 M. Ahmed and I. Dincer, *Int. J. Hydrogen Energy*, 2019, **44**, 2474–2507.

17 H. Kato, K. Asakura and A. Kudo, *J. Am. Chem. Soc.*, 2003, **125**, 3082–3089.

18 Y. Sakata, Y. Matsuda, T. Yanagida, K. Hirata, H. Imamura and K. Teramura, *Catal. Lett.*, 2008, **125**, 22–26.

19 K. Shimura and H. Yoshida, *Phys. Chem. Chem. Phys.*, 2012, **14**, 2678–2684.

20 Y. Sakata, T. Hayashi, R. Yasunaga, N. Yanaga and H. Imamura, *Chem. Commun.*, 2015, **51**, 12935–12938.

21 L. Chen, C. Tang, Y. Zheng, E. Skúlason and Y. Jiao, *J. Mater. Chem. A*, 2022, **10**, 5998–6006.

22 H. Sudrajat and T. K. Nguyen, *Optika*, 2020, **223**, 165370.

23 L. Chao, Y. Jin-Liang, Z. Li-Ying and Z. Gang, *Chin. Phys. B*, 2012, **21**, 127104.

24 X. Zhou, E. J. Hensen, R. A. van Santen and C. Li, *Chem. – Eur. J.*, 2014, **20**, 6915–6926.

25 G. Liu, C. Y. Jimmy, G. Q. M. Lu and H.-M. Cheng, *Chem. Commun.*, 2011, **47**, 6763–6783.

26 G. Kresse and J. Hafner, *Phys. Rev. B: Condens. Matter Mater. Phys.*, 1993, **47**, 558–561.

27 G. Kresse and J. Furthmüller, *Phys. Rev. B: Condens. Matter Mater. Phys.*, 1996, **54**, 11169–11186.

28 G. Kresse and D. Joubert, *Phys. Rev. B: Condens. Matter Mater. Phys.*, 1999, **59**, 1758–1775.

29 J. P. Perdew, K. Burke and M. Ernzerhof, *Phys. Rev. Lett.*, 1996, **77**, 3865–3868.

30 J. P. Perdew, K. Burke and M. Ernzerhof, *Phys. Rev. Lett.*, 1997, **78**, 1396–1396.

31 J. Heyd, G. E. Scuseria and M. Ernzerhof, *J. Chem. Phys.*, 2003, **118**, 8207–8215.

32 V. Wang, N. Xu, J.-C. Liu, G. Tang and W.-T. Geng, *Comput. Phys. Commun.*, 2021, **267**, 108033.

33 J. K. Nørskov, J. Rossmeisl, A. Logadottir, L. Lindqvist, J. R. Kitchin, T. Bligaard and H. Jonsson, *J. Phys. Chem. B*, 2004, **108**, 17886–17892.

34 Y.-H. Fang and Z.-P. Liu, *J. Am. Chem. Soc.*, 2010, **132**, 18214–18222.

35 L. Chen, C. Tang, K. Davey, Y. Zheng, Y. Jiao and S.-Z. Qiao, *Chem. Sci.*, 2021, **12**, 8079–8087.

36 Á. Valdés, Z.-W. Qu, G.-J. Kroes, J. Rossmeisl and J. K. Nørskov, *J. Phys. Chem. C*, 2008, **112**, 9872–9879.

37 W. M. Haynes, *CRC handbook of chemistry and physics*, CRC press, 2014.

38 M. J. Tadjer, M. A. Mastro, N. A. Mahadik, M. Currie, V. D. Wheeler, J. A. Freitas, J. D. Greenlee, J. K. Hite, K. D. Hobart and C. R. Eddy, *J. Electron. Mater.*, 2016, **45**, 2031–2037.

39 M. Schubert, R. Korlacki, S. Knight, T. Hofmann, S. Schöche, V. Darakchieva, E. Janzén, B. Monemar, D. Gogova and Q.-T. Thieu, *Phys. Rev. B*, 2016, **93**, 125209.

40 Y. Oshima, E. G. Víllora, Y. Matsushita, S. Yamamoto and K. Shimamura, *J. Appl. Phys.*, 2015, **118**, 085301.

41 X. Wang, Q. Xu, M. Li, S. Shen, X. Wang, Y. Wang, Z. Feng, J. Shi, H. Han and C. Li, *Angew. Chem.*, 2012, **124**, 13266–13269.

42 W. Guo, Y. Guo, H. Dong and X. Zhou, *Phys. Chem. Chem. Phys.*, 2015, **17**, 5817–5825.

43 Y. Ma, X. Zhao, M. Niu, W. Li, X. Wang, C. Zhai, T. Wang, Y. Tang and X. Dai, *RSC Adv.*, 2017, **7**, 4124–4134.

44 T. Zacherle, P. Schmidt and M. Martin, *Phys. Rev. B: Condens. Matter Mater. Phys.*, 2013, **87**, 235206.

45 X. Ma, Y. Zhang, L. Dong and R. Jia, *Results Phys.*, 2017, **7**, 1582–1589.

46 X. Qiu, J. Zhang, H. Dong and X. Zhou, *Theor. Chem. Acc.*, 2017, **136**, 1–7.

47 H. Niu, X. Wan, X. Wang, C. Shao, J. Robertson, Z. Zhang and Y. Guo, *ACS Sustainable Chem. Eng.*, 2021, **9**, 3590–3599.

48 J. Petit and N. H. Nachtrieb, *J. Chem. Phys.*, 1956, **24**, 1027–1028.

49 H. He, R. Orlando, M. A. Blanco, R. Pandey, E. Amzallag, I. Baraille and M. Rérat, *Phys. Rev. B: Condens. Matter Mater. Phys.*, 2006, **74**, 195123.

50 K. Yamaguchi, *Solid State Commun.*, 2004, **131**, 739–744.

51 R. Abe, *J. Photochem. Photobiol., C*, 2010, **11**, 179–209.

52 A. K. Geim and I. V. Grigorieva, *Nature*, 2013, **499**, 419–425.